A Conceptual Model for the Response of Tropical Rainfall to Orbital Variations

TOBIAS BISCHOFF

California Institute of Technology, Pasadena, California

TAPIO SCHNEIDER

California Institute of Technology, Pasadena, California, and Swiss Federal Institute of Technology, Zurich, Switzerland

ANNA NELE MECKLER

University of Bergen, and Bjerknes Centre for Climate Research, Bergen, Norway

(Manuscript received 23 September 2016, in final form 4 June 2017)

ABSTRACT

Tropical rainfall to first order responds to variations in Earth's orbit through shifts of the intertropical convergence zone (ITCZ) and changes in zonally averaged rainfall intensity. Here, a conceptual model is developed that represents both processes and their response to orbital insolation variations. The model predicts the seasonal evolution of tropical rainfall between 30°S and 30°N. Insolation variations impact seasonal rainfall in two different ways: thermodynamically, leading to variations in rainfall intensity through modulation of the water vapor content of the atmosphere; and dynamically, leading to shifts of the ITCZ through modulation of the global atmospheric energy budget. Thermodynamic and dynamic effects act together to shape the annual-mean response of tropical rainfall to changes in Earth's orbit. The model successfully reproduces changes in annual-mean rainfall inferred from paleo-proxies across several glacial–interglacial cycles. It illuminates how orbital precession and variations of Earth's obliquity affect tropical rainfall in distinct ways near the equator and farther away from it, with spectral signatures of precession and obliquity variations that shift with latitude. It also provides explanations for the observed different phasings of rainfall minima and maxima near the equator and away from it. For example, the model reproduces a phase shift of ~10 ka between rainfall records from caves in northern Borneo (4°N) and from China (approximately 30°N). The model suggests that such phase shifts arise through a different weighting of ITCZ shifts and variations in rainfall intensity, thus providing insight into the mechanisms that drive tropical rainfall changes on orbital time scales.

1. Introduction

The interpretation of paleoclimatological precipitation records from sediment cores or stalagmites is a difficult task. Not only does their interpretation depend on complex isotopic fractionation processes, among other things; understanding how any inferred precipitation variations arise mechanistically also remains a challenge. The amount of precipitation that falls at a given location depends on the water vapor content of the atmosphere and the strength of the atmospheric circulations that transport this water vapor to the location (e.g., Clement et al. 2004; Hsu et al. 2010; Merlis et al. 2013). The water vapor content of the atmosphere can change thermodynamically, primarily through temperature-dependent changes in saturation vapor pressure (Held and Soden 2006; Schneider et al. 2010). Atmospheric circulations can change dynamically, for example by shifting or changing their strength. Any model that attempts to capture how precipitation variations arise, for example, on the time scales of variations in Earth's orbit must therefore include a representation of the salient thermodynamic and dynamic processes.

Previously, variations of tropical precipitation on orbital time scales have often been related to the variations

Corresponding author: Tapio Schneider, tapio@caltech.edu

DOI: 10.1175/JCLI-D-16-0691.1

in local or high-latitude insolation induced by orbital variations (e.g., Cheng et al. 2012; Tachikawa et al. 2014), based on the idea that either local insolation directly impacts precipitation at a given site or high-latitude climate has remote influences on the precipitation distribution in the tropics. For example, precipitation variations on precessional time scales in Brazil and China are out of phase because summer insolation in the Northern Hemisphere is more intense when perihelion occurs in boreal summer, causing strengthened monsoon precipitation over Asia, while summer insolation in the Southern Hemisphere then is reduced, causing weaker monsoon precipitation over Brazil (e.g., Cruz et al. 2005; Cheng et al. 2012; Merlis et al. 2013). This leads to out-of-phase precipitation variations on precessional time scales in the northern and southern subtropics.

In this paper, we present a conceptual model that captures how tropical precipitation and its seasonal cycle respond thermodynamically and dynamically to insolation variations. The model is based on the assumption that tropical precipitation changes primarily 1) because precipitation intensity changes thermodynamically in response to tropical insolation variations, which modulate the water vapor content of the atmosphere, and 2) because the precipitation field as a whole shifts dynamically in latitude, in response to differential global insolation variations that can shift the intertropical convergence zone (ITCZ). The model allows for these two types of changes through a precipitation intensity factor, which is controlled locally by tropical insolation, and through a shape function for the distribution of precipitation with latitude, which encodes the ITCZ latitude and width and depends on the insolation distribution globally.

Previous modeling studies have focused on general circulation model (GCM) simulations that either compare two different climate scenarios (e.g., high vs low obliquity or June vs December perihelion) or use accelerated orbital variations to study the seasonality of tropical precipitation (e.g., Kutzbach 1981; Kutzbach and Guetter 1986; Joussaume et al. 1999; Clement et al. 2004; Kutzbach et al. 2008; Khon et al. 2010; Pausata et al. 2011; Merlis et al. 2013; Tigchelaar and Timmermann 2016). The main benefit of these models lies in the fact that they can incorporate realistic continental boundary conditions and clouds, among other things. Complexity, however, comes at a cost in analytic tractability and computational speed. The main virtue of our conceptual model is that it can be analyzed analytically and that it can be simulated at low computational cost, allowing us to illuminate mechanisms of tropical precipitation variations such as those that have been inferred from paleorecords. We use the model to reproduce annual-mean precipitation variations over the past 350 ka that have been inferred from paleorecords at different latitudes, shedding light on various features of the inferred precipitation variations, such as their phase relation between different latitudes. For example, precipitation variations inferred from caves in northern Borneo at approximately 4°N (Partin et al. 2007; Carolin et al. 2013, 2016) are phase-shifted by around 10 ka relative to precipitation variations inferred from the Hulu, Sanbao, and Linzhu Caves in China at around 30°N (Wang et al. 2001, 2008; Cheng et al. 2009). Our conceptual model provides an explanation of how such phase shifts can arise as a result of the different relative importance of orbital ITCZ shifts and rainfall intensity changes at different latitudes.

Section 2 lays out the details of the precipitation model. Section 3 discusses how different orbital variations (e.g., precession and obliquity variations) affect precipitation in the model and compares our model hindcasts with low-latitude precipitation records spanning the past 350 ka. Section 4 summarizes the results.

2. Model

The precipitation model uses top-of-atmosphere insolation as the only input. This requires simplifying assumptions (e.g., about cloud feedbacks) but leads to a conceptual model that illuminates mechanisms. Our goal is to incorporate just enough complexity to be able to understand orbital changes of precipitation in the annual mean as they are captured in paleoclimatological precipitation records for the tropics (e.g., Wang et al. 2001; Koutavas and Lynch-Stieglitz 2004; Cruz et al. 2005; Partin et al. 2007; Wang et al. 2008; Carolin et al. 2013; Cheng et al. 2012; Tachikawa et al. 2014; Carolin et al. 2016).

Previously, theoretical analyses of paleoclimatological precipitation records for the tropics have resorted to ad hoc arguments that invoke insolation at a specific time of year, either at a high latitude or near the location where the precipitation record is taken (e.g., Wang et al. 2001, 2008; Cheng et al. 2012). Problems with this approach include, for example, that when insolation at the record's site when the ITCZ is overhead in the present climate is taken as determinative of precipitation, this local insolation is not the only important factor determining annual-mean precipitation at a given location. Remote insolation changes can impact the ITCZ location and the timing of ITCZ passage at a location through the global energy balance of the atmosphere (e.g., Chiang and Bitz 2005; Kang et al. 2008, 2009; Donohoe et al. 2013; Schneider et al. 2014). Thus, insolation variations across the globe, including at

remote locations, can impact annual-mean precipitation at tropical locations.

Here, we adopt a different perspective with a simple nonlinear precipitation model that uses insolation globally as input and represents both thermodynamic and dynamic factors. In the model, the precipitation field is independent of longitude and is represented as

$$P(\phi,\lambda,T) = e^{\log[P(\phi,\lambda,T)]} = e^{f(\phi,\lambda,T)}, \tag{1}$$

where ϕ denotes latitude, λ is solar longitude, T is geological time (kiloyears before the present), and $f(\phi, \lambda, T) = \log[P(\phi, \lambda, T)]$ encodes how precipitation varies with latitude ϕ, time of year (expressed by solar longitude λ), and geological time T. The geological time T encapsulates all information about the state of Earth's orbit, which is characterized by the orbital parameters longitude of perihelion ϖ, eccentricity e, and obliquity γ. By expanding $f(\phi, \lambda, T)$ to second order around the latitude of maximum tropical precipitation ϕ_m, where the ITCZ is located, and neglecting higher-order contributions, the precipitation field can approximately be written as the Gaussian

$$P(\phi, \lambda, T) \approx P(\phi_m, \lambda, T)\exp[-(\phi - \phi_m)^2/(2\sigma^2)] \tag{2a}$$

$$= \mathcal{M} \times \mathcal{S}. \tag{2b}$$

We take the variance $\sigma^2 = [\partial_{\phi\phi} f(\phi, \lambda, T)|_{\phi=\phi_m}]^{-1}$ of the precipitation distribution with latitude to be constant for all values of λ and T. This amounts to assuming that the width of the ITCZ is fixed over seasonal and orbital cycles, which is not entirely accurate (Byrne and Schneider 2016) but is a useful first approximation. With these assumptions, the precipitation field (2) can be decomposed into an intensity factor $\mathcal{M} \equiv P(\phi_m, \lambda, T)$ and a Gaussian shape factor $\mathcal{S} = \exp[-(\phi - \phi_m)^2/(2\sigma^2)]$. They depend on the ITCZ latitude $\phi_m(\lambda, T)$, which varies on seasonal and geological time scales, and on the variance of the precipitation distribution σ^2 with latitude. Changes in precipitation $\Delta P = P - P_{\text{ref}}$ relative to a reference distribution P_{ref} as the orbital configuration (T) varies can now be attributed to changes in intensity $\mathcal{M}$ and shape $\mathcal{S}$ via the approximation (neglecting products of intensity changes and ITCZ shifts)

$$\Delta P \approx \underbrace{\mathcal{S}_{\text{ref}}(\Delta\mathcal{M})_{\phi_{m,\text{ref}}}}_{\text{intensity changes}} + \underbrace{\mathcal{S}_{\text{ref}}(\Delta\mathcal{M})_{\phi_{m,T}} + \mathcal{M}_{\text{ref}}\Delta\mathcal{S}}_{\text{ITCZ shifts}}. \tag{3}$$

Since $\phi_m = \phi_m(\lambda, T)$ can be a function of the orbital parameters T, the subscript $\phi_{m,\text{ref}}$ denotes that ϕ_m is taken to be at the reference climate and changes in ϕ_m due to changes in T are neglected. The subscript $\phi_{m,T}$ denotes that changes in T enter indirectly through the influence of T on ϕ_m. The perturbation expansion (3) captures many aspects of the seasonal cycle at individual locations or in longitude sectors in the tropics, such as the characteristic two annual precipitation maxima where the ITCZ is overhead twice a year; however, significant discrepancies to the modern seasonal cycle also exist (e.g., where zonal anomalies in climate play a substantial role, such as over the Americas). Here our focus is on annual-mean changes over orbital time scales, which can be obtained by averaging the precipitation variations (3) over a year.

We use top-of-atmosphere insolation to parameterize the intensity factor $\mathcal{M}$ as proportional to local insolation at the ITCZ latitude ϕ_m. The rationale for this parameterization is that insolation in the deep tropics sets the precipitation intensity thermodynamically through its control on tropical water vapor content (Merlis et al. 2013). The latitude of the ITCZ ϕ_m in the model is parameterized as proportional to the difference in area-integrated insolation between the Northern and Southern Hemisphere. This parameterization assumes that the hemispheric insolation difference alone controls the cross-equatorial atmospheric energy flux, and that the ITCZ position is proportional to the cross-equatorial energy flux (e.g., Kang et al. 2008, 2009; Donohoe et al. 2013; Bischoff and Schneider 2014, 2016; Schneider et al. 2014). We neglect an explicit contribution of a cross-equatorial ocean heat flux component, but it can be viewed as subsumed in the proportionality constant between ITCZ position and hemispheric insolation difference.

a. Precipitation intensity

The intensity factor $\mathcal{M}$ represents the thermodynamic effects of changes in atmospheric water vapor content on precipitation intensity. Atmospheric water vapor content depends primarily on temperature through the saturation vapor pressure because atmospheric relative humidity, especially over oceans, is energetically constrained to change little as the climate changes (Boer 1993; Held and Soden 2000; O'Gorman and Schneider 2008; Schneider et al. 2010). Temperature, in turn, depends primarily on insolation (Huybers and Denton 2008) and is fairly homogeneous across the tropics (Charney 1963; Sobel et al. 2001). So the intensity factor can be assumed to depend only on insolation at the location of maximum precipitation, $S(\phi_m, \lambda, T)$, so that insolation at the location of the ITCZ drives the amount of rain that falls.

To gain insight into how the intensity factor $\mathcal{M}$ varies with insolation at the location of maximum precipitation, we expand it to first order about a reference value of insolation S_{ref},

$$\mathcal{M} \approx P_0 + \alpha[S(\phi_m, \lambda, T) - S_{\text{ref}}], \tag{4}$$

which is justified because seasonal and orbital insolation variations around the equator are generally small. Here, P_0 is a reference precipitation intensity, and $\alpha = \partial P/\partial S|_{S=S_{\text{ref}}} > 0$ defines the sensitivity of precipitation P to variations in insolation at the location of maximum precipitation $S(\phi_m, \lambda, T)$. (Similar linear approximations have been implicitly or explicitly made in many paleoclimatological studies.) If insolation $S(\phi_m, \lambda, T)$ in this expression is evaluated at the equator (i.e., if one takes $\phi_m = 0$), the resulting annual-mean precipitation variations in the model are essentially the same as those obtained with a dynamically varying ϕ_m. However, using the seasonally varying ϕ_m is important to capture the seasonal cycle, for example, with its characteristic double peak where the ITCZ is overhead twice a year (see Fig. 1). We present the result from a model that uses insolation at the equator instead of insolation at the location of the ITCZ in appendix C to illustrate that our results are not strongly dependent on this particular modeling choice.

b. ITCZ latitude

The shape factor $\mathcal{S} = \exp[-(\phi - \phi_m)^2/(2\sigma^2)]$ depends on the ITCZ latitude ϕ_m; the width σ is taken to be fixed. So we need to derive an approximation of the ITCZ latitude ϕ_m in terms of insolation S. We can do this by relating the ITCZ latitude to the cross-equatorial energy flux F_0 (e.g., Broccoli et al. 2006; Kang et al. 2008; Frierson et al. 2013; Donohoe et al. 2013; Bischoff and Schneider 2014). This relation can be expressed as

$$\phi_m \propto -F_0(\lambda - \Delta\lambda, T), \tag{5}$$

where $\Delta\lambda$ is a phase delay between changes in ϕ_m and changes in F_0 (Donohoe et al. 2013; Adam et al. 2016). The ITCZ latitude ϕ_m is related to the cross-equatorial atmospheric energy transport because when the ITCZ moves away from the equator, the cross-equatorial atmospheric circulation strengthens, transporting more energy from the warmer to the colder hemisphere or, more precisely, from the hemisphere with net atmospheric energy input to the hemisphere with net atmospheric energy loss (Kang et al. 2008, 2009; Frierson et al. 2013; Donohoe et al. 2013). To approximate the ITCZ latitude ϕ_m in terms of S, we assume that the cross-equatorial energy flux F_0 is proportional to the hemispheric difference in area-weighted insolation, which leads to

$$\phi_m(\lambda) \approx \beta \left[\int_0^{\pi/2} \cos(\phi) S(\phi, \lambda - \Delta\lambda, T)\, d\phi - \int_{-\pi/2}^{0} \cos(\phi) S(\phi, \lambda - \Delta\lambda, T)\, d\phi \right]. \tag{6}$$

TABLE 1. Parameter values for simulations with precipitation model.

Parameter	Value
P_0	10
S_{ref}	400 W m^{-2}
α	0.075 W^{-1} m^2 mm day^{-1}
β	0.066 W^{-1} m^2
σ	5.0°
$\Delta\lambda$	60°

Here, β is a parameter that measures the sensitivity of the ITCZ latitude ϕ_m to the hemispheric difference in area-averaged insolation. We make the simplifying assumption that the sensitivity β of the ITCZ latitude to the integrated hemispheric insolation difference is constant. However, Bischoff and Schneider (2014, 2016) and Adam et al. (2016) showed that this sensitivity is not constant but depends on the net energy input to the atmosphere near the equator. This would imply that β is, to first order, a linear function of insolation at the equator. If β were taken to be linear in equatorial insolation, like the intensity factor $\mathcal{M}$, it would not substantially impact the model results, only the interpretation of parameters: to first order in eccentricity e, it would amount to a modification of ϕ_m that is small if the sensitivity β only weakly depends on equatorial insolation.

The model specified by (2), (4), and (6) depends only on insolation as input and on the parameters P_0, S_{ref}, α, β, σ, and $\Delta\lambda$. It was used to generate the numerical solutions discussed in what follows, with the parameters listed in Table 1. The parameters P_0, S_{ref}, α, and σ are chosen to obtain realistic zonal-mean precipitation values and shapes for the present-day values of the orbital parameters (Fig. 2). The values for β and $\Delta\lambda$ are chosen to reflect ITCZ location sensitivities similar to the ones found in Donohoe et al. (2013, 2014) and Bischoff and Schneider (2014). For example, the model implies a maximum ITCZ excursion away from the equator to the latitude $\phi_{m,\max} = \beta S_0 \gamma/2$, to first order in obliquity γ (see appendix A); with our parameter values, this gives a maximum ITCZ excursion of $\phi_{m,\max} = 18.4°$, in rough agreement with seasonal ITCZ migrations in regions of stronger ITCZ variations (Schneider et al. 2014). The intensity factor $\mathcal{M}$ with our choice of parameters also captures essential elements of the present-day seasonal cycle of maximum tropical precipitation in a sector over Africa (Fig. 1). However, no extensive parameter tuning was performed, and the results presented in this paper are not very sensitive to the exact values of the model parameters. We have neglected other factors that can also contribute to tropical

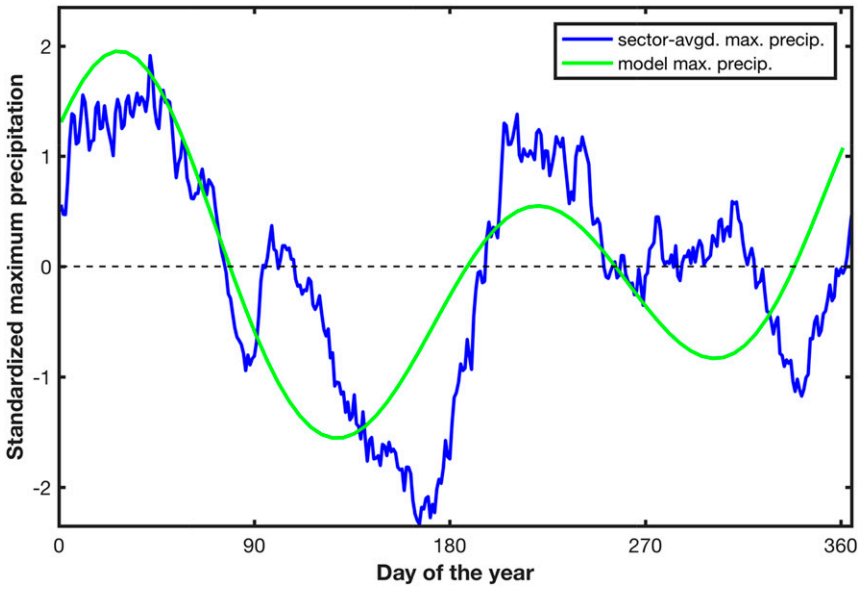

FIG. 1. Comparison of the intensity factor $\mathcal{M}$ (green line) for Earth's present-day orbital configuration with climatological mean (1900–2000) daily data for the seasonal cycle of maximum tropical precipitation (blue line) for a zonal sector over Africa (10°–45°E) from the Twentieth Century Reanalysis Project (Compo et al. 2011). The figure shows the standardized quantities for the year. The model and data both display a characteristic semiannual periodicity.

rainfall changes. For example, our model does not take into account the presence of a deep oceanic overturning circulation, which has been found to affect the zonal- and annual-mean location of the ITCZ (e.g., Frierson et al. 2013; Marshall et al. 2014). The effect of such a circulation can be included in our model, contributing an additional term on the right-hand side of (6). This can affect precipitation changes ΔP through modifications of $\mathcal{S}_{\text{ref}}$ in (3) but not through the perturbation components $\Delta\mathcal{M}$ and $\Delta\mathcal{S}$ (provided the ocean circulation strength does not change appreciably). We found that including such an effect in (6) does not change our results for perturbations around the present climate substantially, even though it is an important factor in shaping the present climate.

3. Response to orbital variations

We illustrate the properties of our model with two representative experiments and compare its hindcasts with tropical precipitation variations inferred from the paleo-record.

a. Results and discussion

Figure 2 shows the model output for two different values of Earth's longitude of perihelion: for perihelion occurring in December (Earth's current perihelion), and in June. The precession response of annual-mean precipitation in our model arises from two effects. First, boreal summer insolation reaches a maximum in the Northern Hemisphere when perihelion precesses from December to June, with correspondingly weakened insolation during austral summer in the Southern Hemisphere. This impacts annual-mean precipitation through changes in rainfall intensity and shifts in the ITCZ location. On the other hand, changes in the duration of the seasons (e.g., boreal summer is shortest when perihelion occurs in June, because Earth orbits more rapidly around the sun when it is closer to it) also lead to seasonal ITCZ shifts and concomitant precipitation changes.

The total precipitation changes broken down into intensity changes and changes due to shifts in the ITCZ according to (3) are shown in Fig. 3. In the annual mean, although annually averaged insolation at each latitude is the same in both simulations, precipitation is enhanced in the subtropics of the hemisphere that receives the more intense summer insolation and is reduced near the equator [see Liu and Schneider (2016) for an example of a different planetary climate where this does not occur]. The changes in annual-mean precipitation arise because, in our model, precipitation is a nonlinear function of local insolation. Thermodynamic changes in precipitation intensity occur because the intensity factor

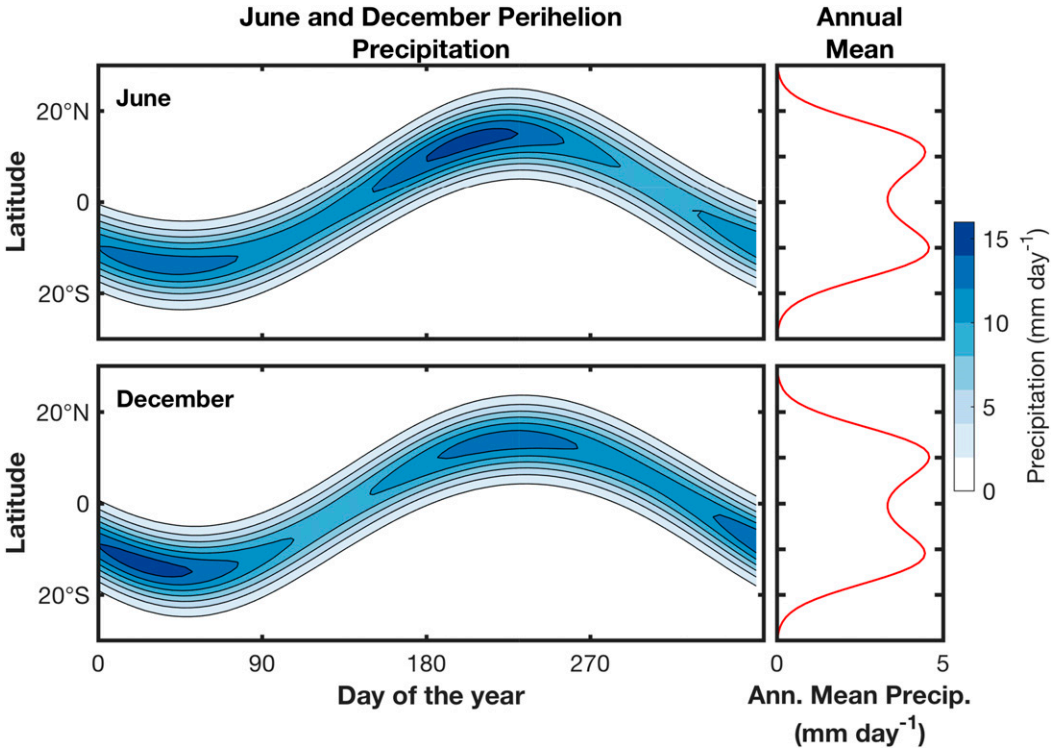

FIG. 2. Precipitation for two different values of longitude of perihelion ϖ (December and June perihelion). Color contours (blue) indicate precipitation with a contour interval of 2.0 mm day^{-1} and a maximum contour at 16 mm day^{-1}. The red curves in the right panels show annual-mean precipitation as a function of latitude. Seasonal maximum precipitation shifts from boreal summer to winter as the longitude of perihelion precesses from June to December. At the same time, in the annual mean, the location of maximum precipitation shifts from the Southern to the Northern Hemisphere due to the nonlinear dependence of the model precipitation on local insolation.

(reflecting water vapor content) is enhanced around the time of perihelion. Because the ITCZ is in the Northern Hemisphere in boreal summer, this leads to a dipole pattern in annual-mean precipitation change as a function of latitude when perihelion precesses from December to June: annual-mean precipitation strengthens in the Northern Hemisphere and weakens in the Southern Hemisphere. The annual-mean precipitation changes although there is no change in annual-mean insolation at a given location because the seasonal cycle of the ITCZ position correlates with the precession-induced seasonal water vapor content changes, leading to nonlinearly rectified changes in the annual mean like those seen in aquaplanet GCM simulations (Merlis et al. 2013).

By contrast, dynamic precipitation changes result from shifts of the ITCZ. These occur because the seasonal migration of the ITCZ into the summer hemisphere progresses farther into the hemisphere with summer perihelion: the ITCZ marches farther into the hemisphere with the brighter (and hence, usually, warmer) summer. This leads to dynamically strengthened precipitation in the northern subtropics during boreal summer when perihelion precesses from December to June, and to weakened precipitation in the southern subtropics during austral summer. On the other hand, changes in the duration of the seasons also lead to shift-induced precipitation changes, causing a dipole pattern during winter. In the annual mean, this results in a double dipole pattern of precipitation changes as a function of latitude, with strengthened precipitation in the northern subtropics, weakened precipitation in the northern deep tropics, and oppositely signed changes in the Southern Hemisphere. Because our model cannot capture zonal variations in precipitation, it should be regarded as a zeroth-order approximation to regions such as the Australo-Asian monsoon sector. For example, in simulations with comprehensive climate models (Clement et al. 2004; Tigchelaar and Timmermann 2016), annual- and zonal-mean precipitation changes do not generally have a double dipole pattern because of zonal inhomogeneities in the precipitation field. Instead, the double dipole is present locally, for example, over Asia and Australia

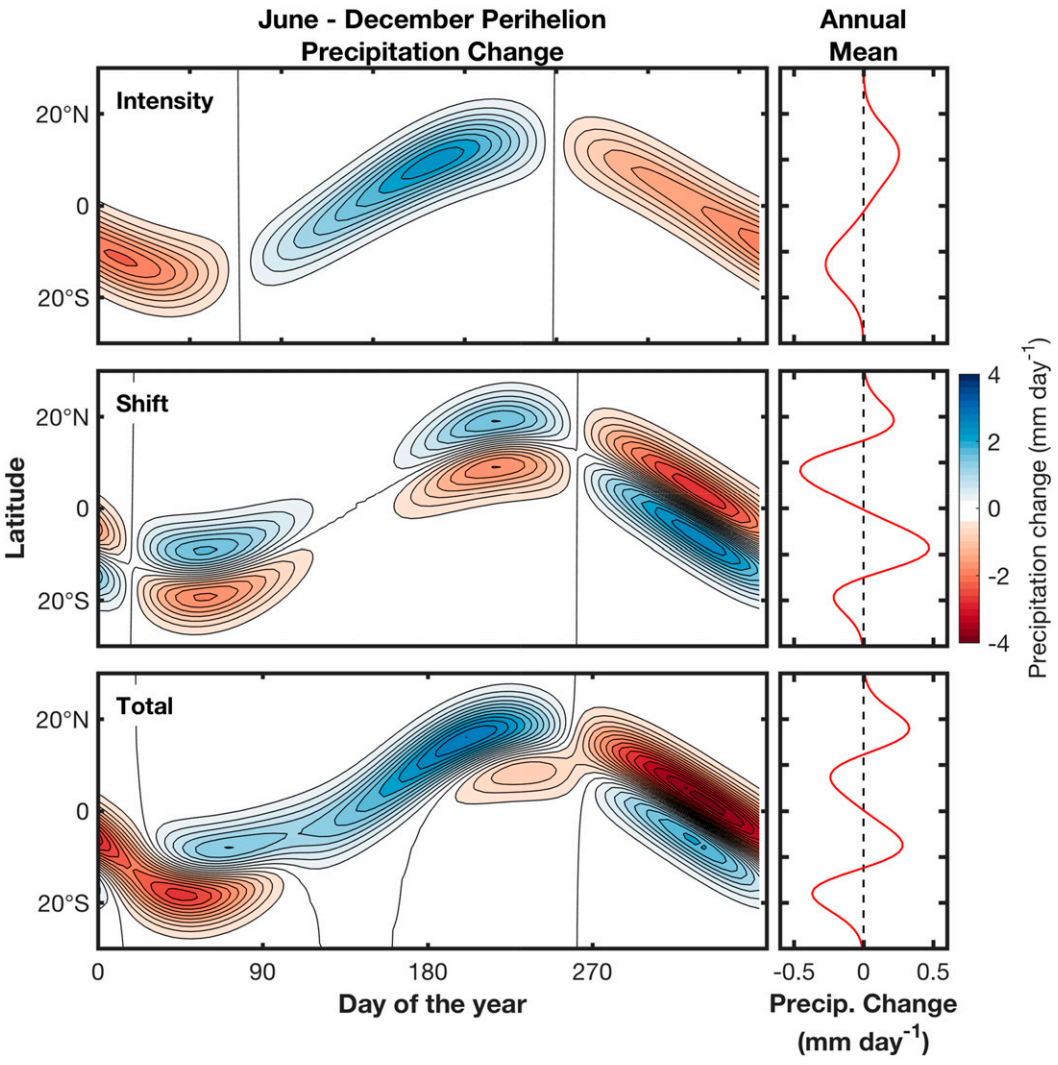

FIG. 3. Precipitation changes, i.e., differences between the panels in Fig. 2, owing to precession (variation in longitude of perihelion ϖ from December to June perihelion). Color contours (blue positive, red negative) indicate precipitation changes, with a contour interval of 0.25 mm day^{-1} and a maximum contour at 4 mm day^{-1}. Perihelion occurs in December for the reference case, as is approximately the case for Earth today. The red curves in the right panels show the change in annual-mean precipitation as a function of latitude. Changes in precipitation intensity reflect the thermodynamically strengthened precipitation in the ITCZ around the time when perihelion occurs. Precipitation changes owing to the ITCZ shift occur because the seasonal migration of the ITCZ progresses farther into the hemisphere with the brighter summer (i.e., with summer perihelion).

(Tigchelaar and Timmermann 2016). The zonal inhomogeneities lead to cancellations in the zonal average; hence, the pattern does not appear in the average.

Figure 4 shows the precipitation changes that occur when Earth's obliquity changes from $\gamma = 24.4°$ to 22.4°. Changes in precipitation intensity in this case are small because near-equatorial insolation changes only weakly when the obliquity varies (the equatorial insolation to first order is independent of obliquity; see appendix B). Because insolation changes under obliquity variations are symmetric about the equator, the annual-mean precipitation changes owing to ITCZ shifts are also symmetric about the equator. Reducing the obliquity weakens the seasonality of insolation. So reducing obliquity weakens annual-mean precipitation in the subtropics dynamically and strengthens it around the equator, because the ITCZ seasonally does not migrate as far poleward for lower obliquities. As a result, total changes in precipitation are dominated by ITCZ shift-induced changes of precipitation.

Figure 5 shows the model prediction as a function of time and latitude split into intensity changes

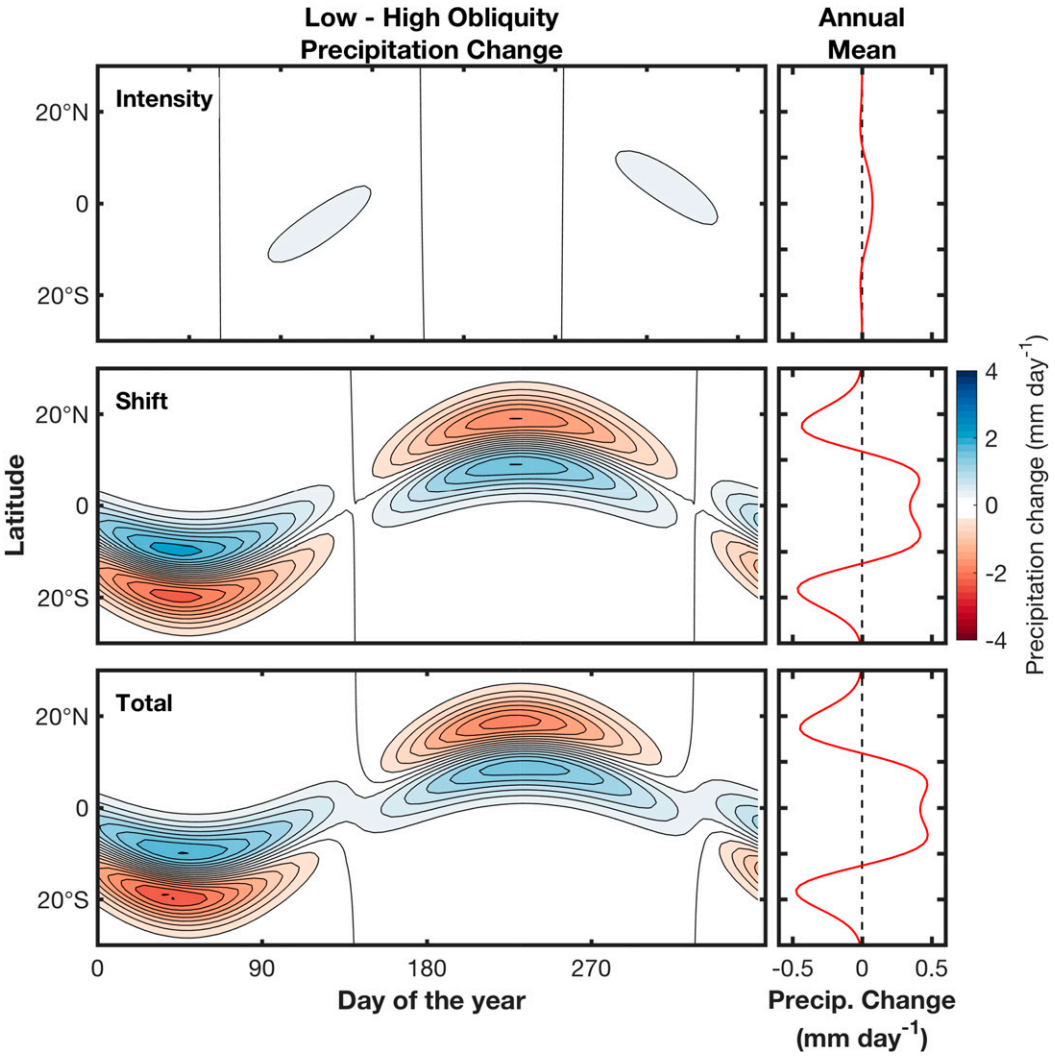

FIG. 4. Precipitation changes owing to changes in Earth's obliquity from $\gamma = 24.4°$ to 22.4°. Color conventions are the same as in Fig. 3. Changes in precipitation intensity are small in this case because near-equatorial insolation changes only weakly when the obliquity varies. Precipitation changes owing to ITCZ shifts are symmetric about the equator because changes in Earth's insolation due to variation in obliquity are symmetric about the equator and are dominated by insolation changes during the solstice seasons.

$\mathcal{S}_{\text{ref}}(\Delta\mathcal{M})_{\phi_{m,\text{ref}}}$ (top row) and changes induced by ITCZ shifts $\mathcal{S}_{\text{ref}}(\Delta\mathcal{M})_{\phi_{m,T}} + \mathcal{M}_{\text{ref}}\Delta\mathcal{S}$ (center row). The dipole and double dipole patterns from Figs. 3 and 4 are again obvious. It is evident from Fig. 5 that phase shifts between subtropical and near-equatorial precipitation emerge through a superposition of intensity and shift-induced changes, leading to a meridional tilt with time of positive and negative anomalies in the total changes (bottom row). Similar phase shifts are also seen in paleoclimate records. The right column in Fig. 5 shows the power spectral density estimates of the model time series. In our model, shift-induced changes introduce a strong obliquity signal in the spectra, especially near the equator. By comparison, obliquity variations lead to only weak intensity changes near the equator because near-equatorial insolation variations induced by obliquity variations are weak (especially compared with subtropical or extratropical insolation variations). At times of relatively low eccentricity (e.g., around 375 ka), precession modulation of precipitation becomes less important and so the importance of intensity variations diminishes (Fig. 5, top); however, obliquity variations are still significant and affect precipitation throughout the tropics through their effect on the ITCZ position (Fig. 5, middle).

b. *Comparison with paleo-records*

The model's response to orbital variations can be compared with proxy-based precipitation records of the

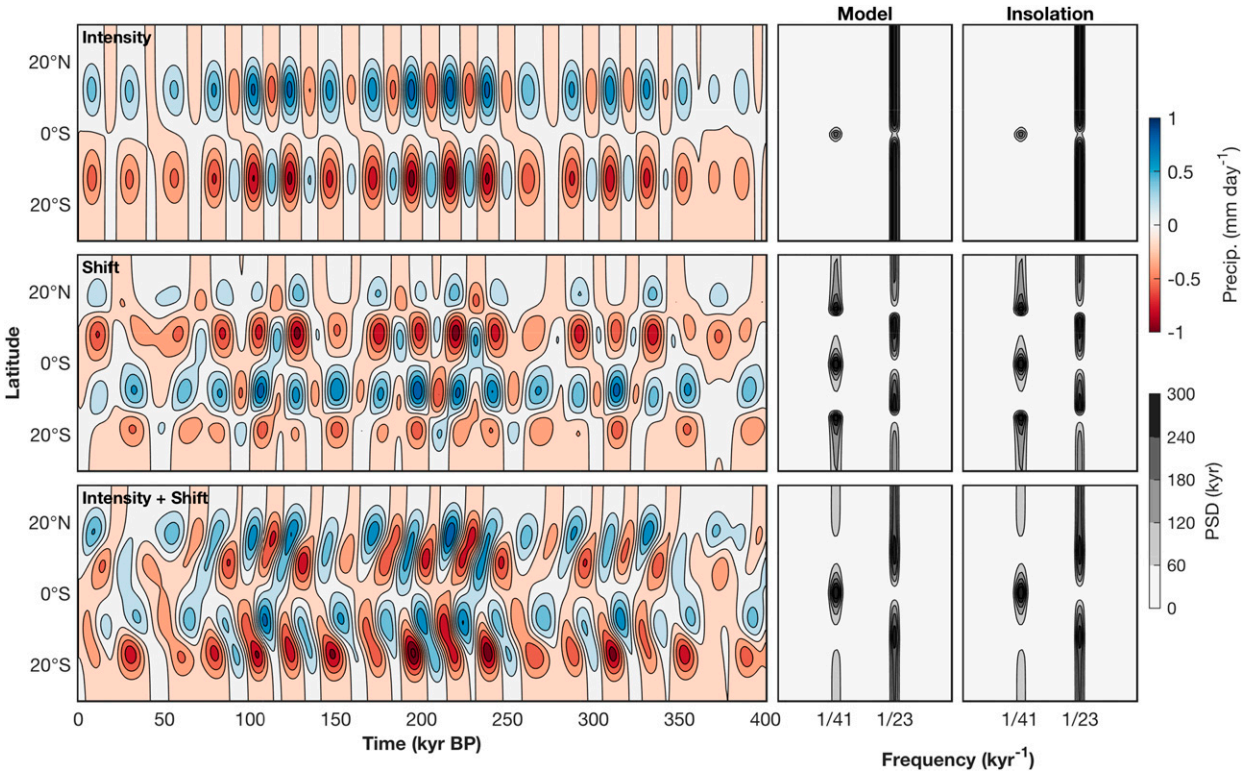

FIG. 5. Changes in annual-mean precipitation (mm day^{-1}) with respect to present-day precipitation. (left) Time series from model output of (top) intensity, (middle) shift, and (bottom) their total. (right) The corresponding Lomb–Scargle (Lomb 1976; Scargle 1982) periodogram power spectral density estimates for the detrended and standardized time series. Precipitation changes due to changes in precipitation intensity and due to shifts in the seasonal cycle of the ITCZ show the characteristic antiphasing between hemispheres, but are almost out of phase with each other near the equator. As a result, the phase lines for changes in total precipitation (intensity + shift) are tilted, which results in a phase lag of subtropical changes compared to near-equatorial changes. The power spectral density estimate is dominated at the 23-kyr precession band but also shows significant power at the 41-kyr obliquity band. Right at the equator, where hemispherically antiphased changes vanish, precipitation changes are driven solely by changes in obliquity.

past 350 ka, which span the Northern and Southern Hemisphere subtropics and tropics. We drive the model with orbital insolation variations for this period (Huybers and Eisenman 2006; Berger 1978; Berger and Loutre 1991). Figure 6 shows the precipitation variations the model produces (black lines), standardized to unit variance, together with paleo-records from China, West Africa, Borneo, Papua New Guinea (PNG), and Brazil (orange/cyan) (Wang et al. 2001; Cruz et al. 2005; Partin et al. 2007; Wang et al. 2008; Cheng et al. 2009; Meckler et al. 2012, 2013; Carolin et al. 2013; Tachikawa et al. 2014; Carolin et al. 2016). The gray vertical bars indicate glacial terminations (Cheng et al. 2009).

The data from China, Borneo, and Brazil are speleothem records. The signal shown is the oxygen isotopic composition (δ^{18}O) of speleothem calcite, interpreted to reflect regional precipitation strength. In some subtropical locations, such as China, the records could however also reflect upstream rainfall closer to the equator (e.g., over India and the Indian Ocean) (e.g., Liu et al. 2014). The speleothem records have been dated radiometrically (with U-Th dating), leading to precise and accurate age control, although precision deteriorates with age. The record from West Africa is based on the Zr content in sediments at Ocean Drilling Site (ODP) Site 658 derived by X-ray fluorescence (XRF) scanning. Zr is used as a proxy for grain size and thus the relative importance of dust input, expected to decrease under wetter conditions. The age model is established for the most part by matching benthic δ^{18}O in the core to the global benthic δ^{18}O stack of Lisiecki and Raymo (2005), and some fine-tuning of sedimentary signals to nearby radiocarbon-dated cores in the uppermost part of the record (Meckler et al. 2013). The Papua New Guinea data are (Ti/Ca) count ratios [plotted as ln(Ti/Ca)] in sediment core MD97–2140, again derived by XRF scanning. The ratio is used as a proxy for terrigenous input to the ocean, interpreted as reflecting river runoff. The record is also dated by oxygen isotope stratigraphy, and

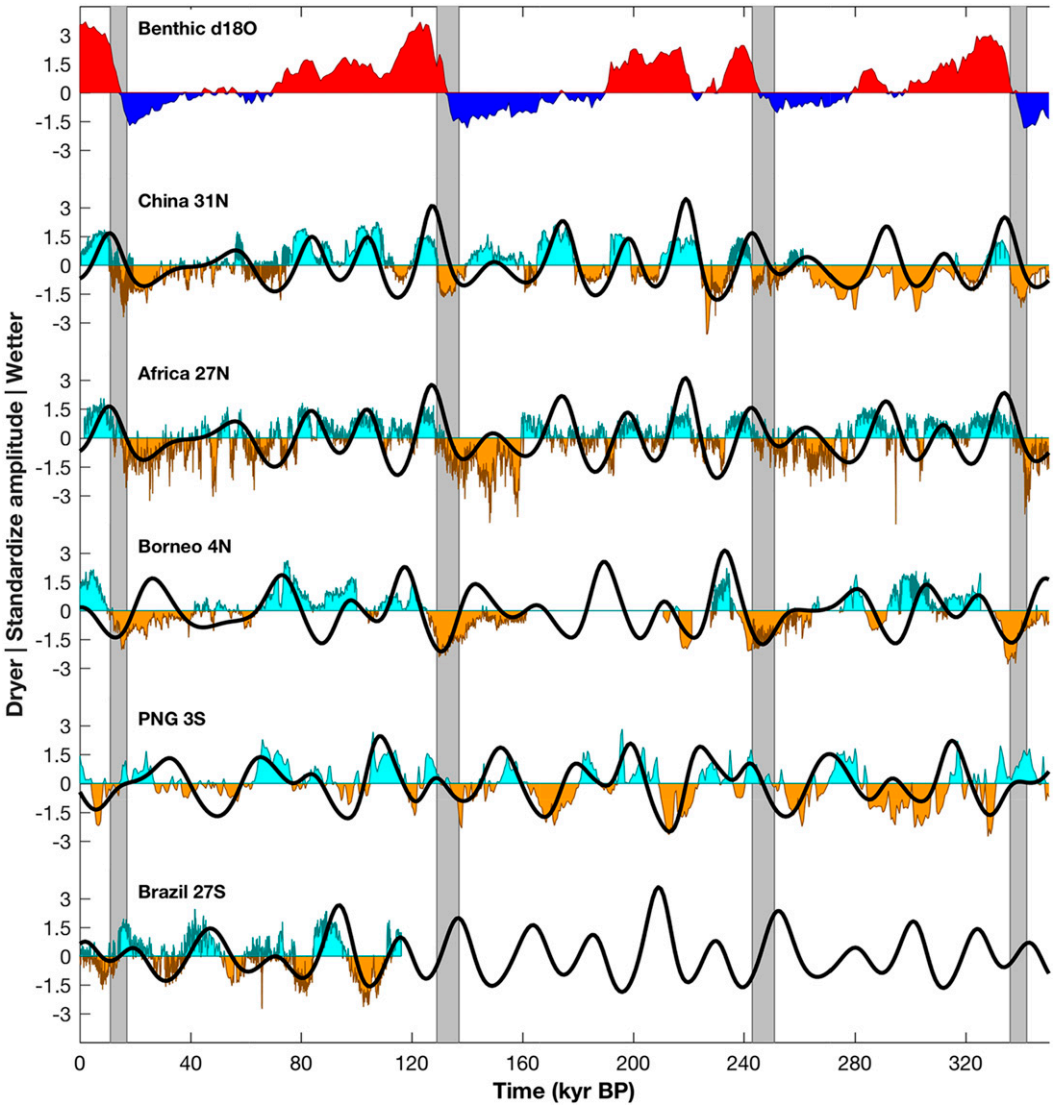

FIG. 6. Comparison of model with precipitation proxies from the paleorecord for the past 350 ka. Colors (orange–cyan) show standardized precipitation proxies, and black lines show the corresponding standardized precipitation variations at the proxy latitude obtained from the model. Gray bars indicate glacial terminations and the uppermost record (red–blue) shows standardized δ^{18}O data from the benthic Lisiecki and Raymo (2005) stack. Eastern China records are from the Hulu, Sanbao, and Linzhu caves (Wang et al. 2001, 2008; Cheng et al. 2009). The African record is from ODP Site 658 (Meckler et al. 2013). The Borneo records are from different caves in Mulu National Park (Partin et al. 2007; Meckler et al. 2012; Carolin et al. 2013, 2016). The Papua New Guinea record is from the sediment core MD97–2140 (Tachikawa et al. 2014). The Brazilian record is from the Botuvera cave (Cruz et al. 2005). All time series are detrended and rescaled to unit variance.

radiocarbon dating in the youngest part (Tachikawa et al. 2014). For comparison, the uppermost record (Fig. 6, red–blue) shows standardized δ^{18}O data from the benthic Lisiecki and Raymo (2005) stack, which reflects a combination of global ice volume and deep-sea temperature and is used here as a rough indication of global-mean temperature variations.

It is evident that the model captures many of the orbital precipitation variations recorded in the paleo-proxies. The agreement is best for subtropical records, where the model is able to capture, for example, the characteristic antiphasing between Chinese and Brazilian records. For subtropical records, the agreement is better for Northern Hemisphere records from China and West Africa, where the model captures the records well for the past 350 ka. For the Brazilian record the agreement is reasonable, but model–data comparisons are hampered by the limited length of the record.

For records from Borneo, the model captures the behavior well between approximately 60 and 160 ka and between 220 and 270 ka, whereas there are substantial model–data discrepancies between 0 and 60 ka. The discrepancies for the past 60 ka cannot be resolved by manipulating the model parameters, which points to effects not captured by our model, such as the zonal variations shown to be important in GCM simulations (Tigchelaar and Timmermann 2016). The model agrees reasonably well with the record from Papua New Guinea, capturing many of the variations over the past 350 ka, although apparently with some phase lags, pointing to factors not considered in our modeling approach.

It is particularly noteworthy that the model captures the phase shift by around 10 ka between precipitation extrema in the subtropical eastern China caves and the equatorial Borneo record. For example, the eastern China cave records (Wang et al. 2001, 2008; Cheng et al. 2009) indicate a precipitation maximum during or immediately after the past four glacial terminations. By contrast, the corresponding precipitation maximum in Borneo (Partin et al. 2007; Meckler et al. 2012; Carolin et al. 2013, 2016) occurs about 10 ka later. It has been suggested that such phase shifts may arise because of the impact of insolation changes on El Niño variability (Carolin et al. 2013, 2016). Our model suggests that even in the absence of El Niño modulations and other zonally varying climate changes, a phase shift between the precipitation variations in the subtropics and deep tropics can occur through the interplay of orbital effects on precipitation intensity (mostly affected by precession) and ITCZ shifts (affected both by precession and obliquity variations).

Figure 7 shows the same records as in Fig. 6 but focusing on the past 160 ka, to see variations in greater detail. The gray lines show standardized insolation curves near the location where the records are taken at the times of the year deemed relevant for local precipitation by the authors of the respective studies (typically, the time of year when the ITCZ is overhead). For the Borneo record (Partin et al. 2007; Carolin et al. 2013, 2016), both our model and the insolation curve used in Carolin et al. (2013, 2016) provide good fits to the data. For the Papua New Guinea record (Tachikawa et al. 2014), our model shows better agreement with the data than the insolation curve used in Tachikawa et al. (2014). For all subtropical records, there is no substantial difference between the commonly used insolation curves and our model. This is because the ITCZ passes overhead only once per year, and precipitation changes in our model are driven primarily by changes in summer insolation, which affect the intensity and the shift component of precipitation similarly in the subtropics. However, an advantage of our physically motivated precipitation model is that it can point to mechanisms of tropical precipitation changes, as the same model applies throughout the low latitudes, whether near the equator or in the subtropics.

Figure 8 shows the power spectral density estimates corresponding to the proxy time series in Figs. 6 and 7 (left column) and the power spectral density estimates for the precipitation model (black lines). Power spectra of representative insolation curves are also shown (red lines, representing spectra of the gray lines in Fig. 7). Almost all proxy time series show significant power at the 23-kyr precession band and at the 41-kyr obliquity band, except for the proxy record from Brazil, which is too short for a 41-kyr peak to be significant. In contrast to insolation curves near the equator, which do not contain significant power in the obliquity band, our precipitation model predicts significant power in the obliquity band even for rainfall records near the equator. The precipitation model predicts significant power at the obliquity band even around the equator because higher-latitude insolation, which is affected by obliquity variations, impacts rainfall near the equator in the annual mean. It does so through ITCZ shifts and changes in timing of the ITCZ passage, as can be seen in Fig. 5 (right column).

For all records shown in Figs. 6–8, our model provides reasonable fits to the inferred standardized precipitation variations, even for sites that are located at very different longitudes. In addition, our model is able to capture the phase shifts between records from different latitudes, such as in the subtropics (China or Brazil) and deep tropics (Borneo or Papua New Guinea). The parameters of the precipitation model were not tuned to provide a best fit to the records shown in the figures. Rough approximations about the dynamic and thermodynamic properties of the atmospheric circulation suffice to generate reasonable agreement between the model and the data.

4. Conclusions

We presented and analyzed an idealized numerical precipitation model for tropical latitudes. The model approximates variations in the local precipitation field using only insolation as input. Even without extensive calibration of the parameters, we find that the model estimate for annual-mean precipitation variations at tropical sites agrees well with standardized paleoclimatological records over the past several hundred thousand years.

More concretely, to study how differences among precipitation records from different latitudes arise, we compared the model output to a set of tropical precipitation records collected near latitudes ranging from

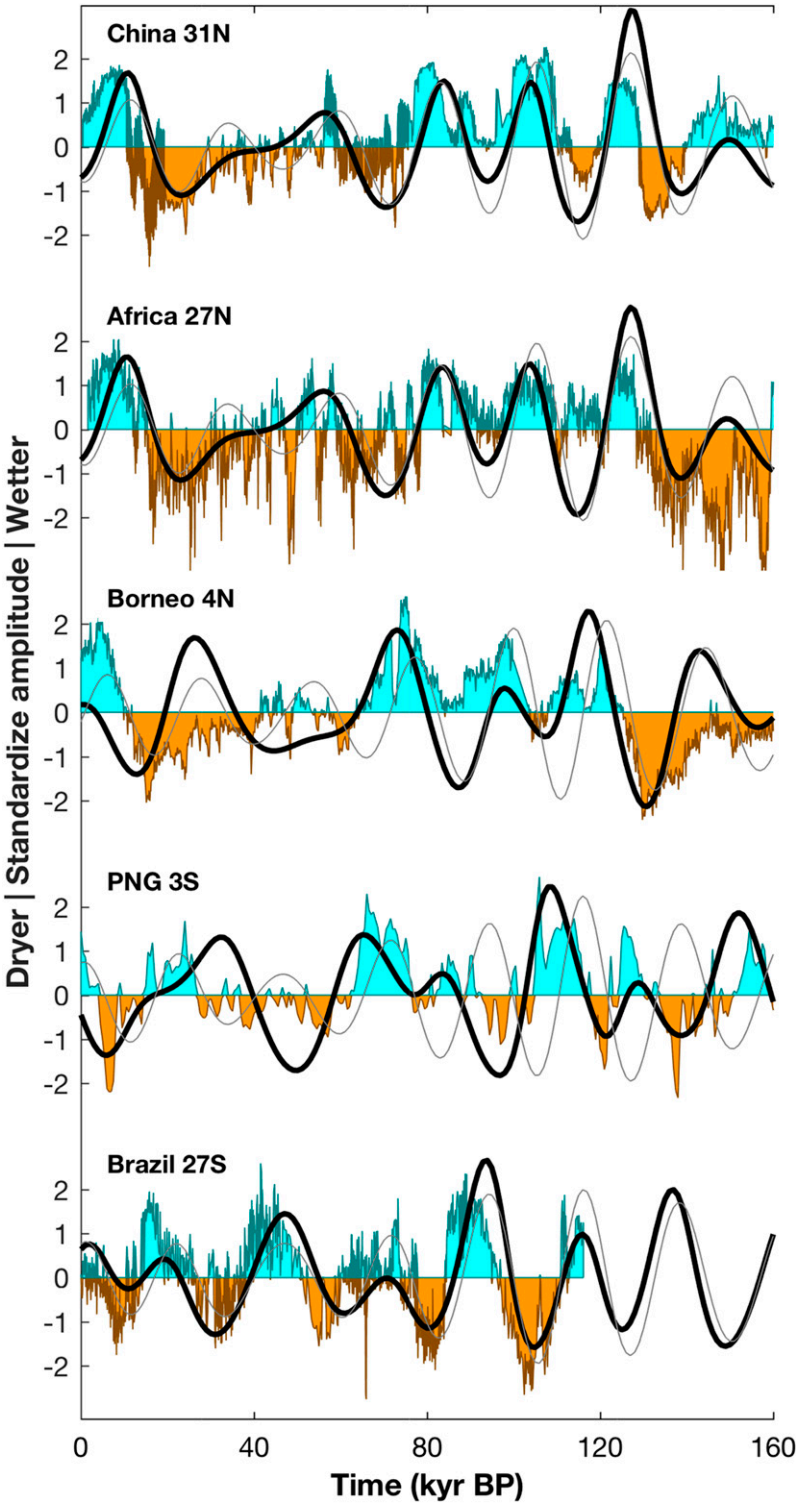

FIG. 7. Comparison of model with precipitation proxies from the paleo-record for the past 160 ka. As in Fig. 6, colors show standardized precipitation proxies, and black lines show the corresponding standardized precipitation variations at the proxy latitude obtained from the model. Gray lines show standardized insolation at 31°N (China), 27°N (Africa), 4°N (Borneo), 3°S [Papua New Guinea (PNG)], and 27°S (Brazil) for solar longitudes 90° (China), 90° (Africa), 180° (Borneo), 270° (PNG), and 270° (Brazil). All time series are detrended and rescaled to unit variance.

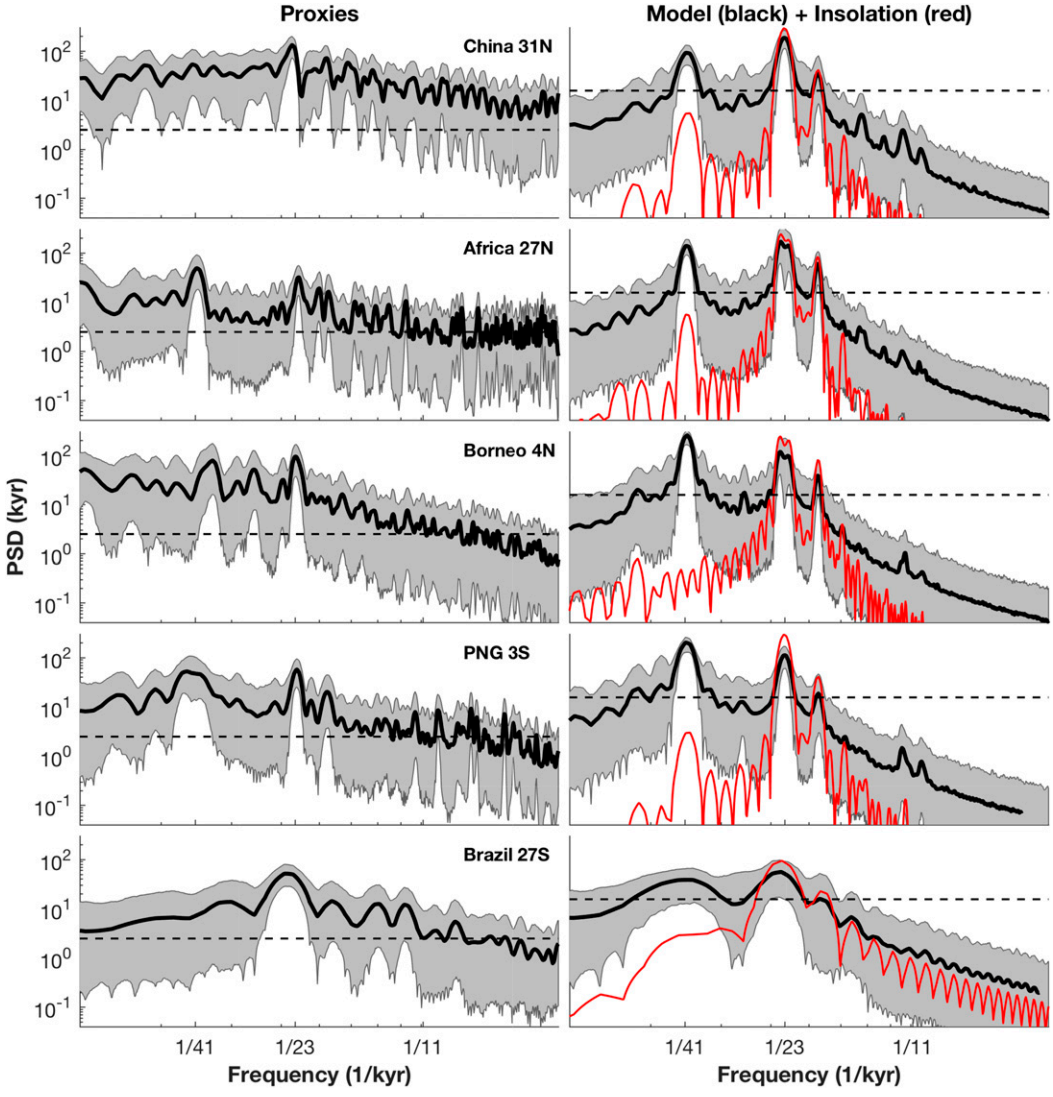

FIG. 8. (left) Spectral density estimates of precipitation proxies from the paleorecord using the standardized and detrended time series from Fig. 6. Solid lines show bootstrap sample mean estimates. Gray areas show 95% bootstrap confidence intervals (see appendix A for details of the method). The black dashed lines show the 95% detection probability threshold. The 23-kyr precession peak is significant in all records, and the 41-kyr obliquity peak is significant in all records but the records from China and Botuvera cave in Brazil. (right) The corresponding spectral density estimates of precipitation model (black lines) based on model time series of the same length at the corresponding proxy time series. The precipitation model was evaluated at 31°N (China), 27°N (Africa), 4°N (Borneo), 3°S (PNG), and 27°S (Brazil). Gray areas again show the 95% confidence interval. Red lines show the spectral density estimate of the standardized insolation curves at the same locations for solar longitudes 90° (China), 90° (Africa), 180° (Borneo), 270° (PNG), and 270° (Brazil).

approximately 30°S to 30°N. We find that our model can capture phase shifts among subtropical precipitation records (Wang et al. 2001; Cruz et al. 2005; Wang et al. 2008; Cheng et al. 2009) and records that were collected from sites near the equator (Partin et al. 2007; Meckler et al. 2012; Carolin et al. 2013, 2016). These phase lags arise because it depends on latitude how important precipitation intensity variations (primarily affected by precession) are relative to ITCZ shifts (affected by both precession and obliquity variations) in their effect on total precipitation variations. As a result, the times when the superposition of intensity variations and ITCZ shifts has maxima and minima vary with latitude (Fig. 5). Additionally, our model is able to explain the spectral power of the proxy records seen at the precession and obliquity bands, showing that ITCZ shifts over the

seasonal cycle can introduce an obliquity signal in near-equatorial precipitation (Fig. 8). This obliquity signal cannot be explained by local equatorial insolation variations alone.

Our results provide a framework in which a wide range of paleoclimatological records can be interpreted mechanistically. For example, it has been suggested that phase shifts among different tropical precipitation records arise due to complex dynamical processes stemming from zonal variations in the oceanic and atmospheric circulations (e.g., Carolin et al. 2013; Tachikawa et al. 2014; Carolin et al. 2016). It is certainly the case that continental configuration and zonal asymmetries in circulations, among other things, play an important role in determining local precipitation and its variations in the tropics. But our relatively simple conceptual model already reproduces phase shifts across latitudes like those inferred from paleo-precipitation records. Zonal variations and regional circulation specifics may be superimposed on this zeroth-order approximation to understand in more detail how tropical precipitation varies on orbital time scales. We propose the precipitation model presented here as a null hypothesis that can be tested with additional tropical precipitation records as they become available. In general, phase lags between records can stem from a variety of sources, and our model makes clear predictions about the frequency content and the phase relationships between different latitudes that result just from insolation changes.

Acknowledgments. We thank Stacy Carolin and Jess Adkins for discussions on the model presented in this paper. We also thank Aaron Donohoe and Zhengyu Liu for helpful reviews of the manuscript. The Geophysical Observational Analysis Tool (http://www.goat-geo.org/) was used to process the 20th-century reanalysis data shown in the appendix. Support for the Twentieth Century Reanalysis Project dataset is provided by the U.S. Department of Energy, Office of Science Innovative and Novel Computational Impact on Theory and Experiment (DOE INCITE) program, and Office of Biological and Environmental Research (BER), and by the National Oceanic and Atmospheric Administration Climate Program Office. This research was partially supported by NSF Grant AGS-1049201, ERC Starting Grant 638467, and by the Bergen Research Foundation.

APPENDIX A

Spectral Density Estimation

Spectral density estimation is performed using the Lomb–Scargle periodogram method (Lomb 1976; Scargle 1982; Horne and Baliunas 1986; Press and Rybicki 1989) for unevenly spaced, detrended, zero-mean, and unit-variance time series. The 95% confidence intervals on the spectral densities are determined via resampling from the original time series using a nonparametric bootstrapping procedure that takes the autocorrelations of the time series into account (Politis and Romano 1994). We resample the original time series by drawing block samples of random length L_i to obtain a new time series of the same length L as the original data time series (for the last block we use a truncation to obtain the correct total length L). The block lengths L_i are drawn from a geometric distribution with probability mass function $p(1-p)^{L_i-1}$, where p is the inverse of the optimal block length for the time series (Politis and White 2004). We draw 1000 bootstrap samples using this procedure and estimate the Lomb–Scargle periodogram for each one of the bootstrap samples to obtain a probability density function at each frequency, which allows us to determine the 95% confidence interval at each frequency. The detection probability is estimated by assuming as null hypothesis that the data are composed of independent Gaussian random variables.

APPENDIX B

Earth's Insolation

To formulate the precipitation model with insolation as input only, we need an analytic formula for Earth's top-of-atmosphere insolation profile. We use the expression

$$S = \frac{S_0}{\pi}\frac{[1+e\cos(\lambda-\varpi)]^2}{(1-e^2)^2}[H_0\sin(\phi)\sin(\delta) + \cos(\phi)\cos(\delta)\sin(H_0)], \tag{B1}$$

where $H_0 = \arccos[-\tan(\phi)\tan(\delta)]$ is the hour angle, $\delta = \arcsin[\sin(\gamma)\sin(\lambda)]$ is the declination angle, and γ is the obliquity of Earth's axis of rotation. Expanding to first order in eccentricity e and obliquity γ, the expression (B1) can be simplified to

$$S \approx \frac{S_0}{\pi}[1+2e\cos(\lambda-\varpi)]\left[\frac{\pi}{2}\gamma\sin(\phi)\sin(\lambda)+\cos(\phi)\right]. \tag{B2}$$

Using the approximation from (B2) instead of (B1) introduces an average error in the annual- and zonal-mean precipitation field of less than 20%. In this approximation, insolation S at the equator is independent of

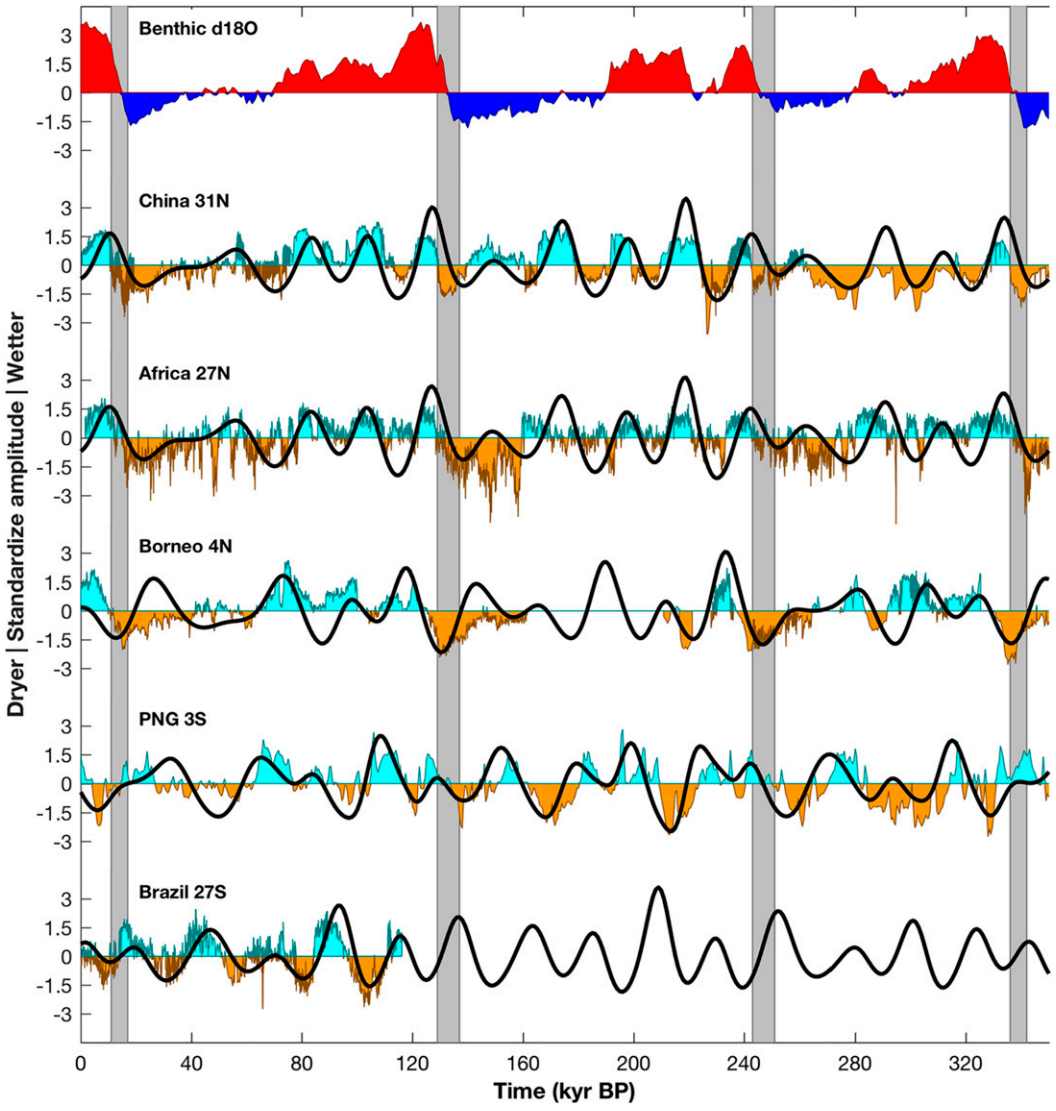

FIG. C1. Comparison of simplified model that uses insolation at the equator to model precipitation intensity with precipitation proxies from the paleorecord for past 350 ka. Plotting conventions are as in Fig. 6.

obliquity. Using (B2), substituting it into (6), and making the zero-eccentricity approximation yields a maximum ITCZ excursion latitude of

$$\phi_{m,\max} \approx \frac{\beta S_0 \gamma}{2}. \tag{B3}$$

APPENDIX C

Model Results Using Equatorial Insolation

When insolation at the equator is used in the precipitation intensity factor (4) instead of insolation at the location of maximum precipitation, the results for annual-mean precipitation are modified only little. In that case, the intensity factor (4) is modified to

$$\mathcal{M} \approx P_0 + \alpha[S(0,\lambda,T) - S_{\text{ref}}]. \tag{C1}$$

This relation is conceptually simpler because it does not require knowledge of the ITCZ location ϕ_m to calculate an approximation of the precipitation intensity $\mathcal{M}$, so that the intensity $\mathcal{M}$ and shift $\mathcal{S}$ components of our model are cleanly separated. Figure C1 shows the comparison between paleoclimatological records and this simplified model. The overall differences are small because, although important seasonal effects are neglected in the simplification (C1), this does not impact annual-mean precipitation variations.

REFERENCES

Adam, O., T. Bischoff, and T. Schneider, 2016: Seasonal and interannual variations of the energy flux equator and ITCZ. Part I: Zonally averaged ITCZ position. *J. Climate*, **29**, 3219–3230, doi:10.1175/JCLI-D-15-0512.1.

Berger, A., 1978: Long-term variations of daily insolation and quaternary climatic changes. *J. Atmos. Sci.*, **35**, 2362–2367, doi:10.1175/1520-0469(1978)035<2362:LTVODI>2.0.CO;2.

——, and M.-F. Loutre, 1991: Insolation values for the climate of the last 10 million years. *Quat. Sci. Rev.*, **10**, 297–317, doi:10.1016/0277-3791(91)90033-Q.

Bischoff, T., and T. Schneider, 2014: Energetic constraints on the position of the intertropical convergence zone. *J. Climate*, **27**, 4937–4951, doi:10.1175/JCLI-D-13-00650.1.

——, and ——, 2016: The equatorial energy balance, ITCZ position, and double-ITCZ bifurcations. *J. Climate*, **29**, 2997–3013, doi:10.1175/JCLI-D-15-0328.1.

Boer, G., 1993: Climate change and the regulation of the surface moisture and energy budgets. *Climate Dyn.*, **8**, 225–239, doi:10.1007/BF00198617.

Broccoli, A. J., K. A. Dahl, and R. J. Stouffer, 2006: Response of the ITCZ to Northern Hemisphere cooling. *Geophys. Res. Lett.*, **33**, L01702, doi:10.1029/2005GL024546.

Byrne, M. P., and T. Schneider, 2016: Energetic constraints on the width of the intertropical convergence zone. *J. Climate*, **29**, 4709–4721, doi:10.1175/JCLI-D-15-0767.1.

Carolin, S. A., K. M. Cobb, J. F. Adkins, B. Clark, J. L. Conroy, S. Lejau, J. Malang, and A. A. Tuen, 2013: Varied response of western Pacific hydrology to climate forcings over the last glacial period. *Science*, **340**, 1564–1566, doi:10.1126/science.1233797.

——, and Coauthors, 2016: Northern Borneo stalagmite records reveal West Pacific hydroclimate across MIS 5 and 6. *Earth Planet. Sci. Lett.*, **439**, 182–193, doi:10.1016/j.epsl.2016.01.028.

Charney, J. G., 1963: A note on large-scale motions in the tropics. *J. Atmos. Sci.*, **20**, 607–609, doi:10.1175/1520-0469(1963)020<0607:ANOLSM>2.0.CO;2.

Cheng, H., R. L. Edwards, W. S. Broecker, G. H. Denton, X. Kong, Y. Wang, R. Zhang, and X. Wang, 2009: Ice age terminations. *Science*, **326**, 248–252, doi:10.1126/science.1177840.

——, A. Sinha, X. Wang, F. W. Cruz, and R. L. Edwards, 2012: The Global Paleomonsoon as seen through speleothem records from Asia and the Americas. *Climate Dyn.*, **39**, 1045–1062, doi:10.1007/s00382-012-1363-7.

Chiang, J. C. H., and C. M. Bitz, 2005: Influence of high latitude ice cover on the marine intertropical convergence zone. *Climate Dyn.*, **25**, 477–496, doi:10.1007/s00382-005-0040-5.

Clement, A. C., A. Hall, and A. J. Broccoli, 2004: The importance of precessional signals in the tropical climate. *Climate Dyn.*, **22**, 327–341, doi:10.1007/s00382-003-0375-8.

Compo, G. P., and Coauthors, 2011: The Twentieth Century Reanalysis Project. *Quart. J. Roy. Meteor. Soc.*, **137**, 1–28, doi:10.1002/qj.776.

Cruz, F. W., and Coauthors, 2005: Insolation-driven changes in atmospheric circulation over the past 116,000 years in subtropical Brazil. *Nature*, **434**, 63–66, doi:10.1038/nature03365.

Donohoe, A., J. Marshall, D. Ferreira, and D. McGee, 2013: The relationship between ITCZ location and cross-equatorial atmospheric heat transport: From the seasonal cycle to the Last Glacial Maximum. *J. Climate*, **26**, 3597–3618, doi:10.1175/JCLI-D-12-00467.1.

——, D. M. Frierson, and D. S. Battisti, 2014: The effect of ocean mixed layer depth on climate in slab ocean aquaplanet experiments. *Climate Dyn.*, **43**, 1041–1055, doi:10.1007/s00382-013-1843-4.

Frierson, D. M. W., and Coauthors, 2013: Contribution of ocean overturning circulation to tropical rainfall peak in the Northern Hemisphere. *Nat. Geosci.*, **6**, 940–944, doi:10.1038/ngeo1987.

Held, I. M., and B. J. Soden, 2000: Water vapor feedback and global warming. *Annu. Rev. Energy Environ.*, **25**, 441–475, doi:10.1146/annurev.energy.25.1.441.

——, and ——, 2006: Robust responses of the hydrological cycle to global warming. *J. Climate*, **19**, 5686–5699, doi:10.1175/JCLI3990.1.

Horne, J. H., and S. L. Baliunas, 1986: A prescription for period analysis of unevenly sampled time series. *Astrophys. J.*, **302**, 757–763, doi:10.1086/164037.

Hsu, Y.-H., C. Chou, and K.-Y. Wei, 2010: Land–ocean asymmetry of tropical precipitation changes in the mid-Holocene. *J. Climate*, **23**, 4133–4151, doi:10.1175/2010JCLI3392.1.

Huybers, P., and I. Eisenman, 2006: Integrated summer insolation calculations. NOAA/NCDC Paleoclimatology Program, accessed 29 April 2010. [Available online at ftp://ftp.ncdc.noaa.gov/pub/data/paleo/climate_forcing/orbital_variations/huybers2006insolation/huybers2006b.txt.]

——, and G. Denton, 2008: Antarctic temperature at orbital timescales controlled by local summer duration. *Nat. Geosci.*, **1**, 787–792, doi:10.1038/ngeo311.

Joussaume, S., and Coauthors, 1999: Monsoon changes for 6000 years ago: Results of 18 simulations from the Paleoclimate Modeling Intercomparison Project (PMIP). *Geophys. Res. Lett.*, **26**, 859–862, doi:10.1029/1999GL900126.

Kang, S. M., I. M. Held, D. M. W. Frierson, and M. Zhao, 2008: The response of the ITCZ to extratropical thermal forcing: Idealized slab-ocean experiments with a GCM. *J. Climate*, **21**, 3521–3532, doi:10.1175/2007JCLI2146.1.

——, D. M. W. Frierson, and I. M. Held, 2009: The tropical response to extratropical thermal forcing in an idealized GCM: The importance of radiative feedbacks and convective parameterization. *J. Atmos. Sci.*, **66**, 2812–2827, doi:10.1175/2009JAS2924.1.

Khon, V., W. Park, M. Latif, I. Mokhov, and B. Schneider, 2010: Response of the hydrological cycle to orbital and greenhouse gas forcing. *Geophys. Res. Lett.*, **37**, L19705, doi:10.1029/2010GL044377.

Koutavas, A., and J. Lynch-Stieglitz, 2004: Variability of the marine ITCZ over the eastern Pacific during the past 30,000 years: Regional perspective and global context. *The Hadley Circulation: Present, Past, and Future*, H. F. Diaz and R. S. Bradley, Eds., Springer, 347–369.

Kutzbach, J. E., 1981: Monsoon climate of the early Holocene: Climate experiment with the earth's orbital parameters for 9000 years ago. *Science*, **214**, 59–61, doi:10.1126/science.214.4516.59.

——, and P. J. Guetter, 1986: The influence of changing orbital parameters and surface boundary conditions on climate simulations for the past 18,000 years. *J. Atmos. Sci.*, **43**, 1726–1759, doi:10.1175/1520-0469(1986)043<1726:TIOCOP>2.0.CO;2.

——, X. Liu, Z. Liu, and G. Chen, 2008: Simulation of the evolutionary response of global summer monsoons to orbital forcing over the past 280,000 years. *Climate Dyn.*, **30**, 567–579, doi:10.1007/s00382-007-0308-z.

Lisiecki, L. E., and M. E. Raymo, 2005: A Pliocene-Pleistocene stack of 57 globally distributed benthic δ^{18}O records. *Paleoceanography*, **20**, PA1003, doi:10.1029/2004PA001071.

Liu, J., and T. Schneider, 2016: Contrasting responses to orbital precession on Titan and Earth. *Geophys. Res. Lett.*, **43**, 7774–7780, doi:10.1002/2016GL070065.

Liu, Z., and Coauthors, 2014: Chinese cave records and the East Asia summer monsoon. *Quat. Sci. Rev.*, **83**, 115–128, doi:10.1016/j.quascirev.2013.10.021.

Lomb, N. R., 1976: Least-squares frequency analysis of unequally spaced data. *Astrophys. Space Sci.*, **39**, 447–462, doi:10.1007/BF00648343.

Marshall, J., A. Donohoe, D. Ferreira, and D. McGee, 2014: The ocean's role in setting the mean position of the inter-tropical convergence zone. *Climate Dyn.*, **42**, 1967–1979, doi:10.1007/s00382-013-1767-z.

Meckler, A., M. Clarkson, K. Cobb, H. Sodemann, and J. Adkins, 2012: Interglacial hydroclimate in the tropical west Pacific through the Late Pleistocene. *Science*, **336**, 1301–1304, doi:10.1126/science.1218340.

——, and Coauthors, 2013: Deglacial pulses of deep-ocean silicate into the subtropical North Atlantic Ocean. *Nature*, **495**, 495–498, doi:10.1038/nature12006.

Merlis, T. M., T. Schneider, S. Bordoni, and I. Eisenman, 2013: Hadley circulation response to orbital precession. Part I: Aquaplanets. *J. Climate*, **26**, 740–753, doi:10.1175/JCLI-D-11-00716.1.

O'Gorman, P. A., and T. Schneider, 2008: The hydrological cycle over a wide range of climates simulated with an idealized GCM. *J. Climate*, **21**, 3815–3832, doi:10.1175/2007JCLI2065.1.

Partin, J. W., K. M. Cobb, J. F. Adkins, B. Clark, and D. P. Fernandez, 2007: Millennial-scale trends in west Pacific warm pool hydrology since the Last Glacial Maximum. *Nature*, **449**, 452–455, doi:10.1038/nature06164.

Pausata, F. S. R., D. S. Battisti, K. H. Nisancioglu, and C. M. Bitz, 2011: Chinese stalagmite $\delta^{18}O$ controlled by changes in the Indian monsoon during a simulated Heinrich event. *Nat. Geosci.*, **4**, 474–480, doi:10.1038/ngeo1169.

Politis, D. N., and J. P. Romano, 1994: The stationary bootstrap. *J. Amer. Stat. Assoc.*, **89**, 1303–1313, doi:10.1080/01621459.1994.10476870.

——, and H. White, 2004: Automatic block-length selection for the dependent bootstrap. *Econometrics Rev.*, **23**, 53–70, doi:10.1081/ETC-120028836.

Press, W. H., and G. B. Rybicki, 1989: Fast algorithm for spectral analysis of unevenly sampled data. *Astrophys. J.*, **338**, 277–280, doi:10.1086/167197.

Scargle, J. D., 1982: Studies in astronomical time series analysis. II—Statistical aspects of spectral analysis of unevenly spaced data. *Astrophys. J.*, **263**, 835–853, doi:10.1086/160554.

Schneider, T., P. A. O'Gorman, and X. J. Levine, 2010: Water vapor and the dynamics of climate changes. *Rev. Geophys.*, **48**, RG3001, doi:10.1029/2009RG000302.

——, T. Bischoff, and G. H. Haug, 2014: Migrations and dynamics of the intertropical convergence zone. *Nature*, **513**, 45–53, doi:10.1038/nature13636.

Sobel, A. H., J. Nilsson, and L. M. Polvani, 2001: The weak temperature gradient approximation and balanced tropical moisture waves. *J. Atmos. Sci.*, **58**, 3650–3665, doi:10.1175/1520-0469(2001)058<3650:TWTGAA>2.0.CO;2.

Tachikawa, K., A. Timmermann, L. Vidal, C. Sonzogni, and O. E. Timm, 2014: CO_2 radiative forcing and intertropical convergence zone influences on western Pacific warm pool climate over the past 400 ka. *Quat. Sci. Rev.*, **86**, 24–34, doi:10.1016/j.quascirev.2013.12.018.

Tigchelaar, M., and A. Timmermann, 2016: Mechanisms rectifying the annual mean response of tropical Atlantic rainfall to precessional forcing. *Climate Dyn.*, **47**, 271–293, doi:10.1007/s00382-015-2835-3.

Wang, Y., H. Cheng, R. L. Edwards, Z. S. An, J. Y. Wu, C. C. Shen, and J. A. Dorale, 2001: A high-resolution absolute-dated late Pleistocene monsoon record from Hulu Cave, China. *Science*, **294**, 2345–2348, doi:10.1126/science.1064618.

——, and Coauthors, 2008: Millennial- and orbital-scale changes in the East Asian monsoon over the past 224,000 years. *Nature*, **451**, 1090–1093, doi:10.1038/nature06692.